Search for a heavy neutral Higgs boson in a left-right model with an inverse-seesaw mechanism at the LHC

Mustafa Ashry

mustafa@sci.cu.edu.eg

Department of Mathematics, Faculty of Science, Cairo University

Center for Fundamental Physics (CFP), Zewail City of Science and Technology

Based on (e-Print: 2101.08255 [1]) in collaboration with *S. Khalil* and *K. Ezzat*

LHC Higgs Working Group WG3 (BSM) - Extended Higgs Sector subgroup meeting

6-7 June 2021-Online

Outline

Outline

Outline

Outline

Outline

Outline

Outline

Outline

Outline

Outline

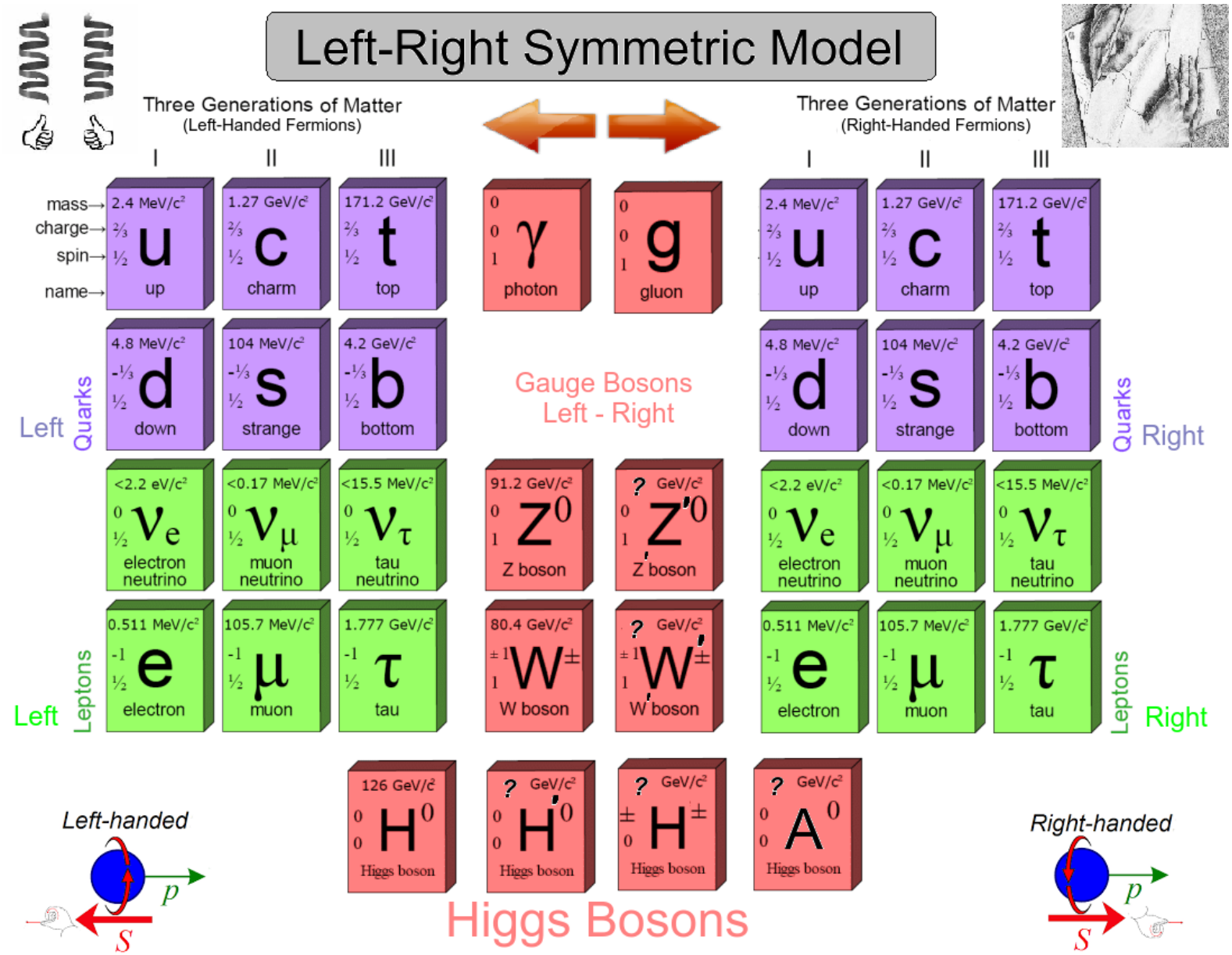
Left-Right Symmetric Model
Three Generations of Matter
(Left-Handed Fermions)
Three Generations of Matter
(Right-Handed Fermions)
I
II
III
mass→
charge→
spin→
name→
2.4 MeV/c²
1.27 GeV/c²
171.2 GeV/c²
u
up
c
charm
t
top
4.8 MeV/c²
104 MeV/c²
4.2 GeV/c²
d
down
s
strange
b
bottom
Left Quarks
Right Quarks
<2.2 eV/c²
<0.17 MeV/c²
<15.5 MeV/c²
νe
electron neutrino
νμ
muon neutrino
ντ
tau neutrino
0.511 MeV/c²
105.7 MeV/c²
1.777 GeV/c²
e
electron
μ
muon
τ
tau
Left Leptons
Right Leptons
γ
photon
g
gluon
Gauge Bosons
Left - Right
91.2 GeV/c²
Z boson
? GeV/c²
Z' boson
80.4 GeV/c²
W±
W boson
W' boson
126 GeV/c²
H⁰
Higgs boson
H'⁰
H±
A⁰
Higgs Bosons
Left-handed
Right-handed
p
S

- The left-right symmetric model is based on the symmetry group

$$SU(3)_C \times SU(2)_L \times SU(2)_R \times U(1)_{B-L}. \tag{1}$$

- In addition to the usual left-right symmetric group and fermion content [2, 3, 4, 5, 6, 7], extra discrete symmetry Z_2 and fermion fields S_1 and S_2 are added to adopt inverse-seesaw mechanism for neutrino masses .
- Moreover, we consider a truly minimal Higgs sector consisting of only one bidoublet and a right-handed doublet for symmetry breaking and spectrum.

Fields	$SU(3)_C \times SU(2)_L \times SU(2)_R \times U_{B-L}$
$Q_L = \begin{pmatrix} u_L \\ d_L \end{pmatrix}$	$(\mathbf{3}, \mathbf{2}, \mathbf{1}, \frac{1}{3})$
$Q_R = \begin{pmatrix} u_R \\ d_R \end{pmatrix}$	$(\mathbf{3}, \mathbf{1}, \mathbf{2}, \frac{1}{3})$
$L_L = \begin{pmatrix} \nu_L \\ e_L \end{pmatrix}$	$(\mathbf{1}, \mathbf{2}, \mathbf{1}, -1)$
$L_R = \begin{pmatrix} \nu_R \\ e_R \end{pmatrix}$	$(\mathbf{1}, \mathbf{1}, \mathbf{2}, -1)$
S_1	$(\mathbf{1}, \mathbf{1}, \mathbf{1}, -2)$
S_2	$(\mathbf{1}, \mathbf{1}, \mathbf{1}, 2)$
$\phi = \begin{pmatrix} \phi_1^0 & \phi_1^+ \\ \phi_2^- & \phi_2^0 \end{pmatrix}$	$(\mathbf{1}, \mathbf{2}, \mathbf{2}, 0)$
$\chi_R = \begin{pmatrix} \chi_R^+ \\ \chi_R^0 \end{pmatrix}$	$(\mathbf{1}, \mathbf{1}, \mathbf{2}, 1)$

Table 1: The LRIS particle Content quantum numbers.

- The Higgs potential is [5]

$$\begin{aligned} V(\phi,\chi_R) &= \mu_1 \mathsf{Tr}(\phi^\dagger\phi) + \mu_2[\mathsf{Tr}(\tilde{\phi}\phi^\dagger) + \mathsf{Tr}(\tilde{\phi}^\dagger\phi)] + \lambda_1(\mathsf{Tr}(\phi^\dagger\phi))^2 \\ &+ \lambda_2[(\mathsf{Tr}(\tilde{\phi}\phi^\dagger))^2 + (\mathsf{Tr}(\tilde{\phi}^\dagger\phi))^2] + \lambda_3 \mathsf{Tr}(\tilde{\phi}\phi^\dagger)\mathsf{Tr}(\tilde{\phi}^\dagger\phi) \\ &+ \lambda_4 \mathsf{Tr}(\phi\phi^\dagger)(\mathsf{Tr}(\tilde{\phi}\phi^\dagger) + \mathsf{Tr}(\tilde{\phi}^\dagger\phi)) + \mu_3(\chi_R^\dagger\chi_R) + \rho_1(\chi_R^\dagger\chi_R)^2 \\ &+ \alpha_1 \mathsf{Tr}(\phi^\dagger\phi)(\chi_R^\dagger\chi_R) + \alpha_2(\chi_R^\dagger\phi^\dagger\phi\chi_R) + \alpha_3(\chi_R^\dagger\tilde{\phi}^\dagger\tilde{\phi}\chi_R) \\ &+ \alpha_4(\chi_R^\dagger\phi^\dagger\tilde{\phi}\chi_R + h.c.). \end{aligned} \tag{2}$$

- The Yukawa Lagrangian

$$\begin{aligned} \mathcal{L}_{\mathsf{Y}} &= \sum_{i,j=1}^{3} y_{ij}^L \bar{L}_{Li}\phi L_{Rj} + \tilde{y}_{ij}^L \bar{L}_{Li}\tilde{\phi} L_{Rj} + y_{ij}^Q \bar{Q}_{Li}\phi Q_{Rj} + \tilde{y}_{ij}^Q \bar{Q}_{Li}\tilde{\phi} Q_{Rj} \\ &+ y_{ij}^s \bar{L}_{Ri}\tilde{\chi}_R S_{2j}^c + h.c., \end{aligned} \tag{3}$$

- The complete electroweak symmetry breaking pattern of the LRIS is accomplished in the following two stages

$$SU(2)_L \times SU(2)_R \times U(1)_{B-L} \xrightarrow{\langle \chi_R \rangle} SU(2)_L \times U(1)_Y \xrightarrow{\langle \phi \rangle} U(1)_{\mathsf{em}} \quad (4)$$

where

$$\langle \chi_R \rangle = v_R, \quad \langle \phi \rangle = \mathsf{diag}(k_1, k_2). \quad (5)$$

- The hypercharge is defined by the formula

$$Y = T_R^3 + \frac{B-L}{2}. \quad (6)$$

- The neutral gauge matrix $(W^3_{R\mu}, V_\mu, W^3_{L\mu})$and $Z - Z'$ mixing are

$$M^2_{ZZ'} = \frac{1}{4}\begin{pmatrix} g_R^2(v_R^2 + v^2) & -g_{BL}g_R v_R^2 & -g_L g_R v^2 \\ . & g_{BL}^2 v_R^2 & 0 \\ . & . & g_L^2 v^2 \end{pmatrix}, \tag{7}$$

$$\tan 2\vartheta = \frac{2g_2^3\sqrt{g_2^2 + 2g_{BL}^2}}{(g_2^2 + g_{BL}^2)^2(\frac{v_R}{v})^2 - 2g_2^2 g_{BL}^2}. \tag{8}$$

- The charged gauge matrix $(W^\pm_{L\mu}, W^\pm_{R\mu})$ and $W - W'$ mixing are

$$M^2_{WW'} = \frac{1}{4}\begin{pmatrix} g_L^2 v^2 & -g_L g_R v^2 s_{2\beta} \\ . & g_R^2(v^2 + v_R^2) \end{pmatrix}, \tag{9}$$

$$\tan 2\xi = \frac{2g_L g_R s_{2\beta}}{g_R^2(1 + (\frac{v_R}{v})^2) - g_L^2}. \tag{10}$$

- $M_{W,W'}$ are approximately $M_W = g_2 v/2,\ M_{W'} = (g_2/2)\sqrt{v^2 + v_R^2}$).

- The Dirac mass matrices for the SM fermions

$$M_u = \frac{v}{\sqrt{2}}(y^Q s_\beta + \tilde{y}^Q c_\beta), \tag{11}$$

$$M_d = \frac{v}{\sqrt{2}}(y^Q c_\beta + \tilde{y}^Q s_\beta), \tag{12}$$

$$M_\ell = \frac{v}{\sqrt{2}}(y^L c_\beta + \tilde{y}^L s_\beta). \tag{13}$$

- The physical fermions' masses are

$$M_u^{\text{diag}} = V_L^{u\dagger} M_u V_R^u, \quad M_d^{\text{diag}} = V_L^{d\dagger} M_d V_R^d, \quad M_\ell^{\text{diag}} = V_L^{\ell\dagger} M_\ell V_R^\ell . \tag{14}$$

- The left and right CKM quark mixing matrices are

$$V_{L,R} = V_{L,R}^{u\dagger} V_{L,R}^d. \tag{15}$$

- After $B-L$ symmetry breaking, a small mass term $\mu_s \bar{S}_2^c S_2$ (and plausibly $\mu_s' \bar{S}_1^c S_1$) is generated from a non-renormalizable term (of dimension seven at least $\propto \chi_R^4 \bar{S}_2^c S_2/M^3$), which implies that $\mu_s = \lambda_s v_R^4/M^3 \lesssim \mathcal{O}(1)$ KeV [8]
- The the standard neutrino IS mechanism [9, 10] neutrino masses Lagrangian is

$$\mathcal{L}_m^\nu = M_D \bar{\nu}_L \nu_R + M_R \bar{\nu}_R^c S_2 + \mu_s \bar{S}_2^c S_2 + h.c., \tag{16}$$

where $M_D = v(y^L s_\beta + \tilde{y}^L c_\beta)/\sqrt{2}$ is the Dirac neutrino mass matrix and $M_R = y^s v_R/\sqrt{2}$.

- The neutrino mass matrix can be written as $\bar{\psi}^c \mathcal{M}_\nu \psi$ with the flavour basis $\psi = (\nu_L^c, \nu_R, S_2)$ and

$$\mathcal{M}_\nu = \begin{pmatrix} 0 & M_D & 0 \\ M_D^T & 0 & M_R \\ 0 & M_R^T & \mu_s \end{pmatrix}. \tag{17}$$

- The physical light and heavy neutrino states $\nu_{\ell_i}, \nu_{h_j},\ i = 1 \ldots 3,\ j = 1 \ldots 6$, with the following mass eigenvalues:

$$m_{\nu_{\ell_i}} = M_D M_R^{-1} \mu_s (M_R^T)^{-1} M_D^T, \quad i = 1 \ldots 3, \tag{18}$$

$$m^2_{\nu_{h_j}} = M_R^2 + M_D^2, \quad j = 1 \ldots 6. \tag{19}$$

- Choices of $\mu_s \sim \mathcal{O}(10^{-7})$ GeV, and $v_R \sim \mathcal{O}(10^3)$ GeV So for $\lambda_s \sim \mathcal{O}(10^{-3})$ we need $M \sim \mathcal{O}(10)$ TeV gives the experimental light neutrino masses.

- Only one physical charged Higgs boson with mass are

$$m^2_{H^\pm} = \frac{\alpha_{32}}{2}\left(\frac{v_R^2}{c_{2\beta}} + v^2 c_{2\beta}\right), \tag{20}$$

  where $\alpha_{32} = \alpha_3 - \alpha_2$.

- Only one physical pseudoscalar Higgs with mass

$$m^2_A = \frac{1}{2}\left(\frac{v_R^2}{c_{2\beta}}\alpha_{32} - 4v^2(2\lambda_2 - \lambda_3)\right). \tag{21}$$

- Finally, we consider the CP-even Higgs bosons. The (3×3) CP-even Higgs bosons mass matrix are

$$m_{11} = 2v^2(\lambda_1 s_\beta^2 + \lambda_{23} c_\beta^2 + \lambda_4 s_{2\beta}) + \frac{1}{4}(\frac{1}{c_{2\beta}} + 1)\alpha_{32} v_R^2, \tag{22}$$

$$m_{12} = m_{21} = v^2((\lambda_1 + \lambda_{23}) s_{2\beta} + 2\lambda_4) - \frac{1}{4}\alpha_{32} v_R^2 t_{2\beta}, \tag{23}$$

$$m_{13} = m_{31} = v v_R(\alpha_{13} s_\beta + \alpha_4 c_\beta), \tag{24}$$

$$m_{22} = 2v^2(\lambda_1 c_\beta^2 + \lambda_{23} s_\beta^2 + \lambda_4 s_{2\beta}) + \frac{1}{4}(\frac{1}{c_{2\beta}} - 1)\alpha_{32} v_R^2, \tag{25}$$

$$m_{23} = m_{32} = v v_R(\alpha_{12} c_\beta + \alpha_4 s_\beta), \tag{26}$$

$$m_{33} = 2\rho_1 v_R^2, \tag{27}$$

  where $\alpha_{1i} = \alpha_1 + \alpha_i,\ i = 2, 3$ and $\lambda_{23} = 2\lambda_2 + \lambda_3$.
- There are three massive scalar Higgs bosons one of which, we took it the lightest, can be the SM-like Higgs boson that we fix its mass with $m_h = 125$ GeV [11, 12].

- The other two eigenvalues are given in terms of the SM-like mass by

$$m^2_{H_{2,3}} = \frac{1}{2}\left(T^h - m_h^2 \mp \sqrt{(T^h - m_h^2)^2 - \frac{4D^h}{m_h^2}}\right), \tag{28}$$

  where the trace $T^h = \mathrm{Tr}(M_H^2)$ and the determinant $D^h = \mathrm{Det}(M_H^2)$.
- The next lightest CP-even neutral Higgs boson, h', could have a mass of order a few hundred GeVs, as shown in Fig. 1 (left) in terms of one of the scalar potential parameters
- Other parameters in the scalar potential, with choosing $\lambda_{23} \in [-0.1, 3]$ and

$$\lambda_1 \in [0.18, 0.30], \quad \lambda_4 \in [0.70, 0.99], \quad \alpha_1 \in [0.06, 0.16], \tag{29}$$

$$\alpha_4 \in [0.60, 0.99], \quad \rho_1 \in [0.08, 0.14]\ . \tag{30}$$

- Fig. 1 (left) shows the mass of the next lightest Higgs boson versus the relevant parameter combination α_{23}.
- Fig. 1 (right) displays the h'-mixing Z^H_{2i} versus $m_{h'}$ where h' is essentially ϕ_1-like with smaller contributions from the real components of ϕ_2 and χ_R.

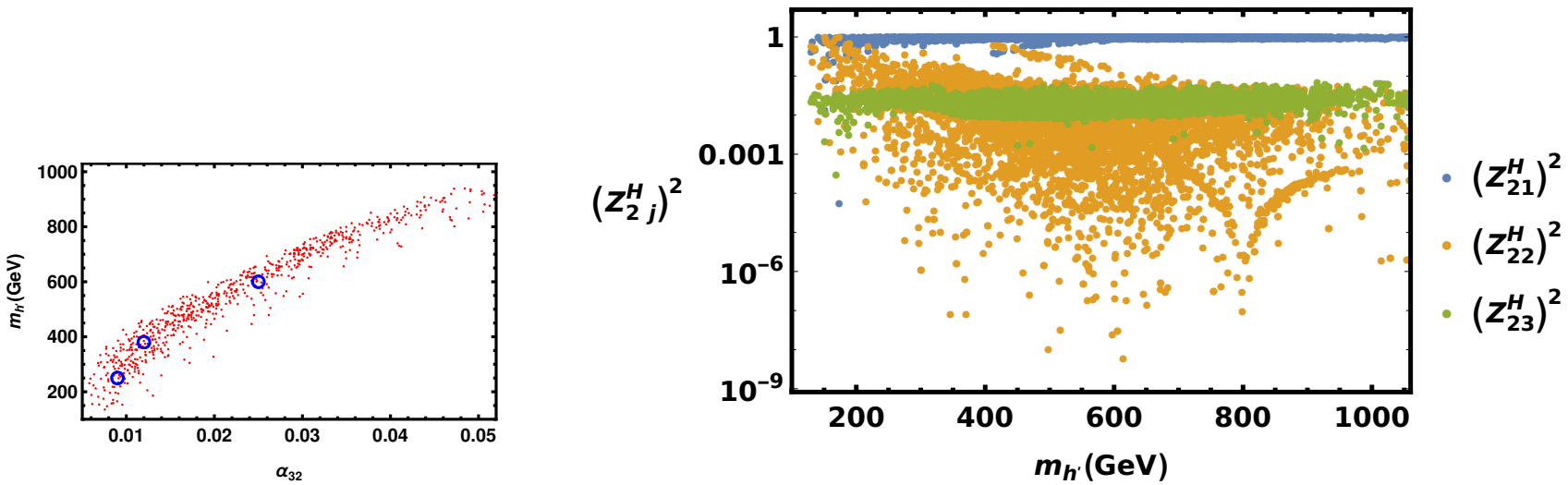

Figure 1: The next lightest Higgs mass (Left) and mixing (right).

- The interaction couplings of h' with Z_μ gauge boson, and with the SM-like Higgs are

$$g_{h'hh} \approx -2iv((\lambda_1 - \lambda_{23})c_\beta + 3\lambda_4 s_\beta) Z_{21}^H (Z_{12}^H)^2, \tag{31}$$

$$g_{h'ZZ} \approx \frac{i}{2} g_2^2 v (c_\beta Z_{21}^H + s_\beta Z_{22}^H)(Z_{32}^Z - Z_{12}^Z)^2, \tag{32}$$

- Numerically, we have $g_{h'ZZ} \sim 60$ GeV and 60 GeV $\lesssim g_{h'hh} \lesssim 150$ GeV. i.e., the coupling $g_{h'ZZ}$ is typically smaller than the coupling $g_{h'hh}$.

Par	α_1	α_2	α_3	α_4	λ_1	λ_2	λ_3	λ_4
BP1	0.133	0.155	0.164	0.833	0.215	0.316	-0.155	0.997
BP2	0.229	0.090	0.102	0.620	0.198	0.230	-0.104	0.917
BP3	0.118	0.168	0.193	0.957	0.228	0.309	-0.116	0.985

Table 2: Benchmark points (BP) and corresponding parameters and Higgs spectrum

ρ_1	t_β	v_R (GeV)	$m_{H^\pm}$ (GeV)	m_A (GeV)	$m_{h'}$ (GeV)	m_{H_3} (GeV)
0.104	0.134	6400	440	315	250	3000
0.117	0.159	6400	430	350	400	3100
0.138	0.055	6400	700	650	600	3400

Table 3: Benchmark points (BP) and corresponding parameters and Higgs spectrum

Z_{11}^H	Z_{12}^H	Z_{13}^H	Z_{21}^H	Z_{22}^H	Z_{23}^H	Z_{31}^H	Z_{32}^H	Z_{33}^H
-0.135	0.989	-0.051	0.978	0.125	-0.166	0.158	0.072	0.985
-0.155	0.987	-0.051	0.982	0.148	-0.119	0.110	0.068	0.992
-0.065	0.997	-0.038	0.988	0.059	-0.141	0.138	0.047	0.989

Table 4: Neutral Higgs mixing corresponding to the three BPs in Tables 2 & 3.

Outline

- The heavy Higgs boson, h', is mainly produced at the LHC from gluon-gluon fusion (ggF) process and Fig. 2 (left) shows the h' ggF-production cross section versus $m_{h'}$.
- Fig. 2 (right) shows the h' decay branching ratios with $m_{h'}$. For $m_{h'} \leq 600$ GeV, BR$(h' \to hh) \geq 10\%$, which gives a hope for probing this heavy Higgs through this channel.

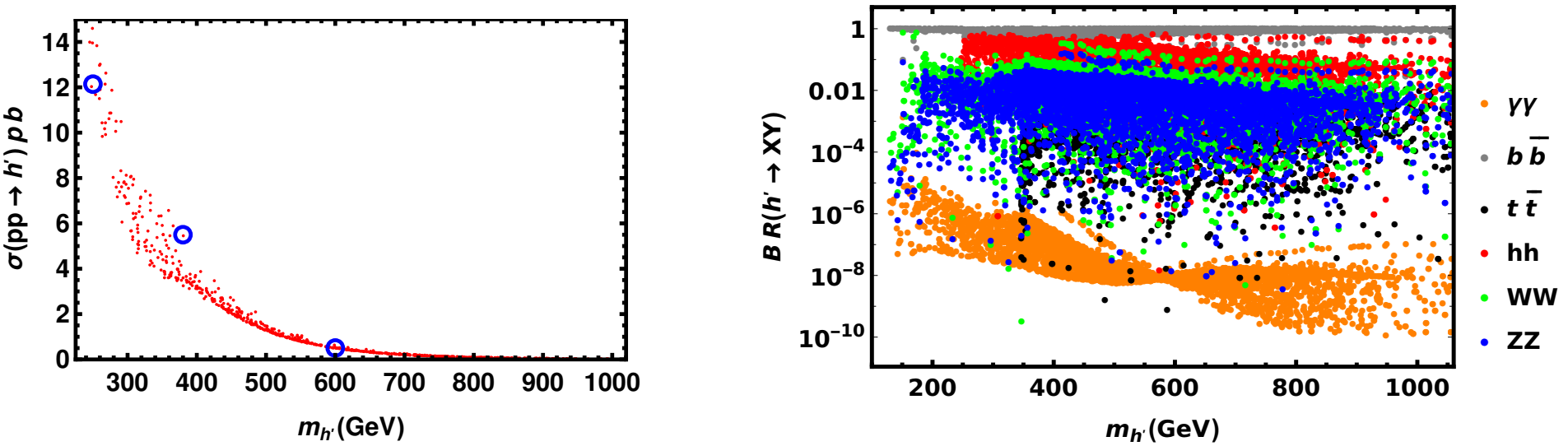

Figure 2: (Left) The h' ggF production cross section with the three BP points circled. (Right) h'-decay branching ratios.

- The cross section $\sigma(pp \to h' \to hh \to b\bar{b}b\bar{b})$ for probing h' at the LHC is large but this process has a huge background and the signal is much lower than the relevant background, even for a quite heavy Higgs boson: $m_{h'} > 600$ GeV [13, 14] as in Fig. 3.
- We looked at the selection cuts for the following events of any combination of the four final states' b jets, respectively: $|\eta_{bb}| < 2.4,\ (P_T)_{bb} > 30.0$ GeV and 100.0 GeV $< M_{bb} < 150.0$ GeV.
- Also, we applied the cuts [13, 14] on $|\eta_b| < 2.5\ (2.4)$ and $(P_T)_b > 40\ (30)$ GeV of each single b jet of the final states.
- We also looked at the decay process $h' \to hh \to 2b + 2W \to bb\ell\nu\ell\nu$, and we found that $\sigma(pp \to h' \to hh \to 2b + 2W \to bb\ell\nu\ell\nu) \sim \mathcal{O}(10^{-15})$ pb. As a result, h' can not be probed through this channel.
- No hope her!

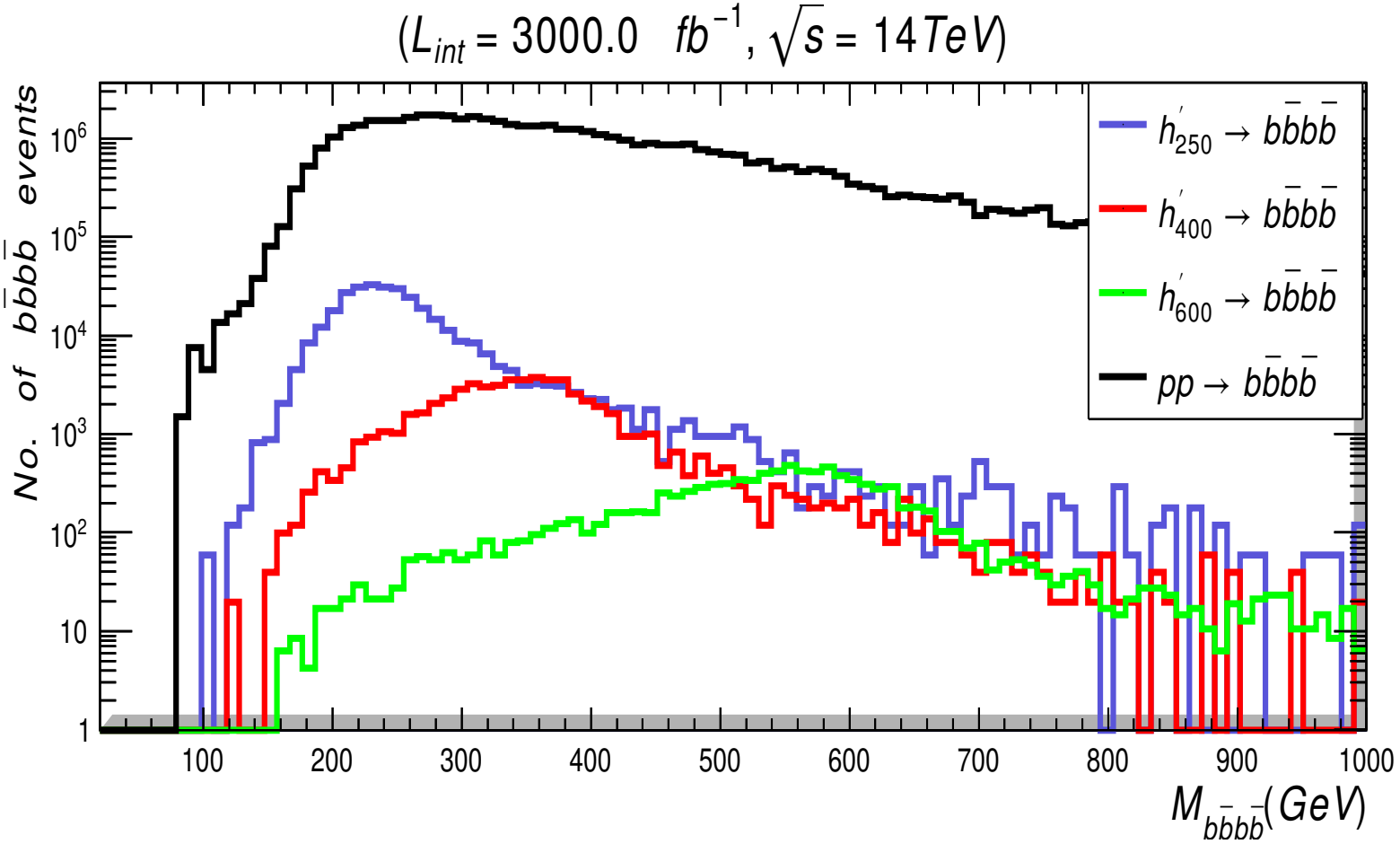

Figure 3: Number of signals events for $h' \to b\bar{b}b\bar{b}$ at $m_{h'} = 250$ GeV (blue) , 400 GeV (red), and 600 GeV (green) induced by the ggF versus $M_{b\bar{b}b\bar{b}}$, at $\sqrt{s} = 14$ TeV and $L_{\text{int}} = 3000$ fb^{-1} with the background events (black) after applying the cut flow $|\eta| < 2.4,\ (P_T)_{bb} > 30.0$ and

- Here we adapt the following different values of h'-mass: $m_{h'} = 250$ GeV, 400 GeV and 600 GeV

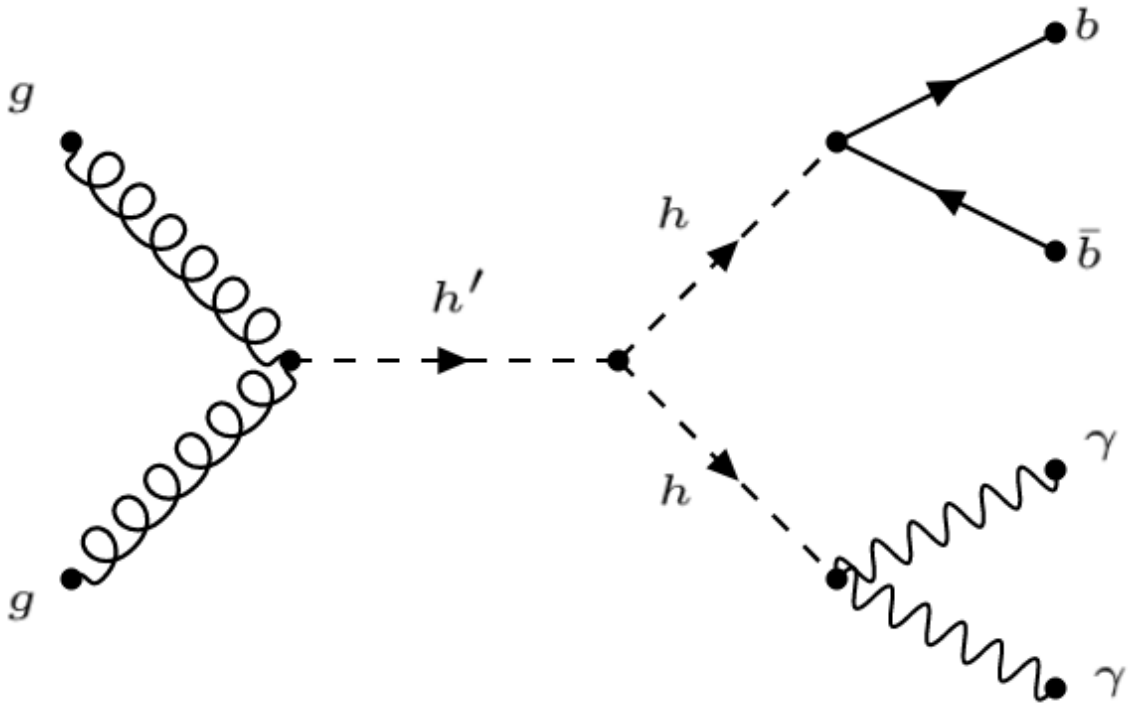

Figure 4: The ggF h'-production and decay $h' \to hh \to b\bar{b}\gamma\gamma$

- We have $\Gamma_{h'}/m_{h'} \ll 1$ and in the narrow width approximation the total cross section $\sigma(pp \to h' \to hh \to b\bar{b}\gamma\gamma)$ is decomposed into

$$\sigma(pp \to h' \to hh \to b\bar{b}\gamma\gamma) \approx \sigma(pp \to h') \times \text{BR}(h' \to hh) \times \text{BR}(h \to b\bar{b}) \times \text{BR}(h \to \gamma\gamma), \tag{33}$$

$m_{h'}$ (GeV)	$\sigma(pp \to h')$ (pb)	BR$(h' \to hh)$	$\sigma(pp \to h' \to hh \to b\bar{b}\gamma\gamma)$ (fb)
250	12.140	0.30	6.30
400	5.050	0.20	1.01
600	0.504	0.18	0.05

Table 5: $pp \to h' \to hh \to b\bar{b}\gamma\gamma$ production and decays for $m_{h'} = 250$ GeV, 400 GeV and 600 GeV.

- The relevant background from the SM processes are

$$pp \to bbh\gamma\gamma/bbja/bbjj/cc\gamma\gamma/ccj\gamma/jj\gamma\gamma/ggh\gamma\gamma/tt/tt\gamma/tth\gamma\gamma/bbz\gamma\gamma/zh\gamma\gamma.$$

- All these backgrounds can be reduced by appropriate kinematics cuts as Tab. 6.

Cuts (Select)	Signal (S): $m_{h'} = 250$ GeV (400 GeV)	Background (B)	S/$\sqrt{\text{B}}$
Initial (no cut)	1904.00 (308.00)	25058.00	12.000 (1.950)
$M_{\gamma\gamma} > 119.5$ GeV	846.70 ± 21.70 (177.95 ± 8.82)	3015.10 ± 51.50	15.419 ± 0.00527 (3.241 ± 0.0
$M_{\gamma\gamma} < 125.0$ GeV	522.00 ± 19.30 (106.60 ± 8.36)	387.40 ± 19.20	26.530 ± 0.01500 (5.419 ± 0.0

Table 6: Cut flow charts for the $h' \to hh \to b\bar{b}\gamma\gamma$ signal versus its relevant background and the corresponding number of events and significance at 300 fb^{-1} and $\sqrt{s} = 14$ TeV for $m_{h'} = 250$ GeV (400 GeV).

- After this cut we can see signal above background

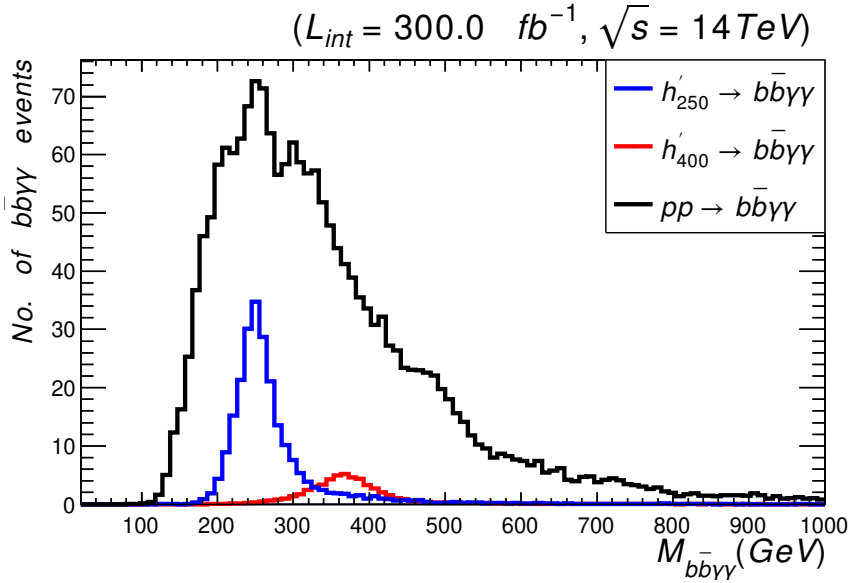

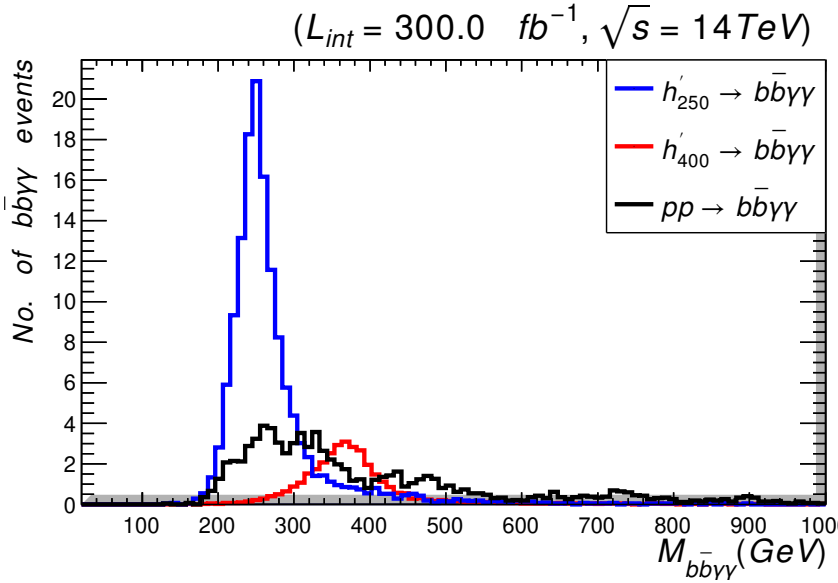

Figure 5: Number of signal events for $h' \to b\bar{b}\gamma\gamma$ decays at mass $m_{h'} = 250$ GeV (blue) and 400 GeV (red) induced by ggF versus the invariant mass of the final states $b\bar{b}\gamma\gamma$, at $\sqrt{s} = 14$ TeV and $L_{\text{int}} = 300$ fb^{-1} alongside with the relevant background events (black) before (left) and after (right) applying the cut flow of Tab. 6. The corresponding vlaues of cross sections and branching ratios are given in Tab. 5.

- With $m_{h'} = 600$ GeV, one must consider higher $L_{\text{int}} \sim 3000$ fb^{-1}, as the associated production and decay cross section are quite small. Here we apply following cut flow.

Cuts (Select)	Signal (S): $m_{h'} = 600$ GeV	Background (B)	S/$\sqrt{\text{B}}$
Initial (no cut)	155.000	250589.00	0.310
$M_{bb} < 200.0$ GeV	52.250 ± 5.18	39823.60 ± 82.40	0.264 ± 0.0008
$M_{\gamma\gamma} > 119.5$ GeV	34.436 ± 5.91	4252.00 ± 64.70	0.530 ± 0.0010
$M_{\gamma\gamma} < 140.0$ GeV	34.432 ± 5.91	1826.60 ± 42.00	0.800 ± 0.0004
$(\Delta R)_{\gamma\gamma} < 2.0$	29.830 ± 4.35	305.20 ± 17.08	1.710 ± 0.0500
$(\Delta R)_{bb} < 2.0$	28.300 ± 4.46	198.63 ± 7.66	2.010 ± 0.0200
$(P_T)_{\gamma\gamma} > 200.0$ GeV	22.160 ± 4.36	60.75 ± 7.70	2.800 ± 0.0260

Table 7: Cut flow charts for the $h' \to hh \to b\bar{b}\gamma\gamma$ signal versus its relevant background and the corresponding number of events and significance at $L_{\text{int}} = 3000$ fb^{-1} and $\sqrt{s} = 14$ TeV for $m_{h'} = 600$ GeV.

- after this cut we can see signal above background

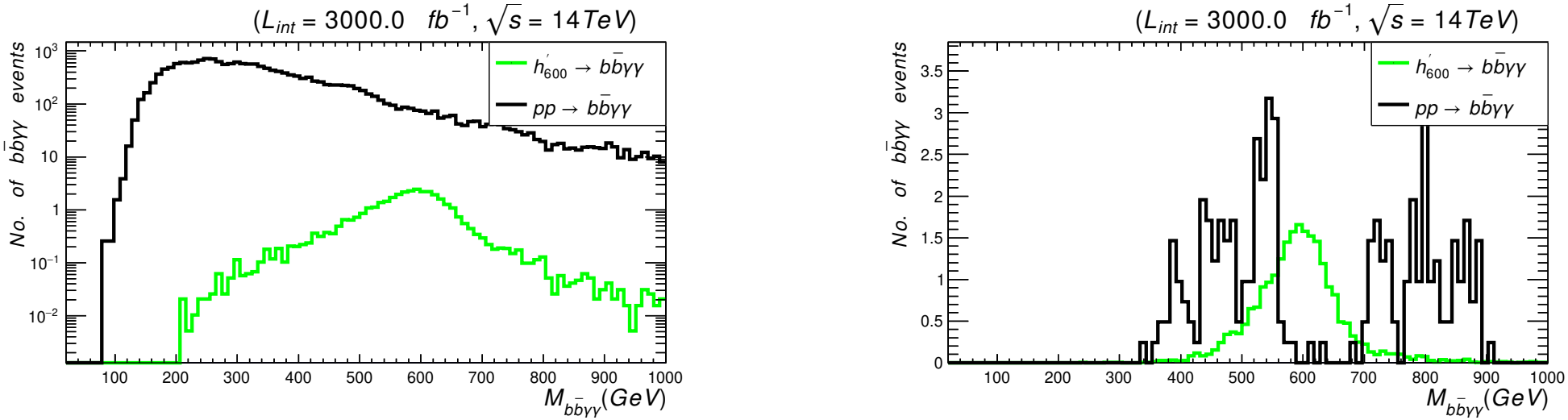

Figure 6: Number of signal events for $h' \to b\bar{b}\gamma\gamma$ decays at mass $m_{h'} = 600$ GeV (green) induced by ggF versus the invariant mass of the final states $b\bar{b}\gamma\gamma$, at $\sqrt{s} = 14$ TeV and $L_{\text{int}} = 3000$ fb^{-1} alongside the relevant background events background (black) before (left) and after (right) applying the cut flow set of Tab. 7. The corresponding values of cross sections and branching ratios are given in Tab. 5. Left pannel is plotten on log-scale vertical axis for the signal to show up relatively.

- According to Fig. 7 and Fig. 6, it is clear that even h' with $m_{h'} \gtrsim 600$ GeV can still be discovered, but at the High-Luminosity

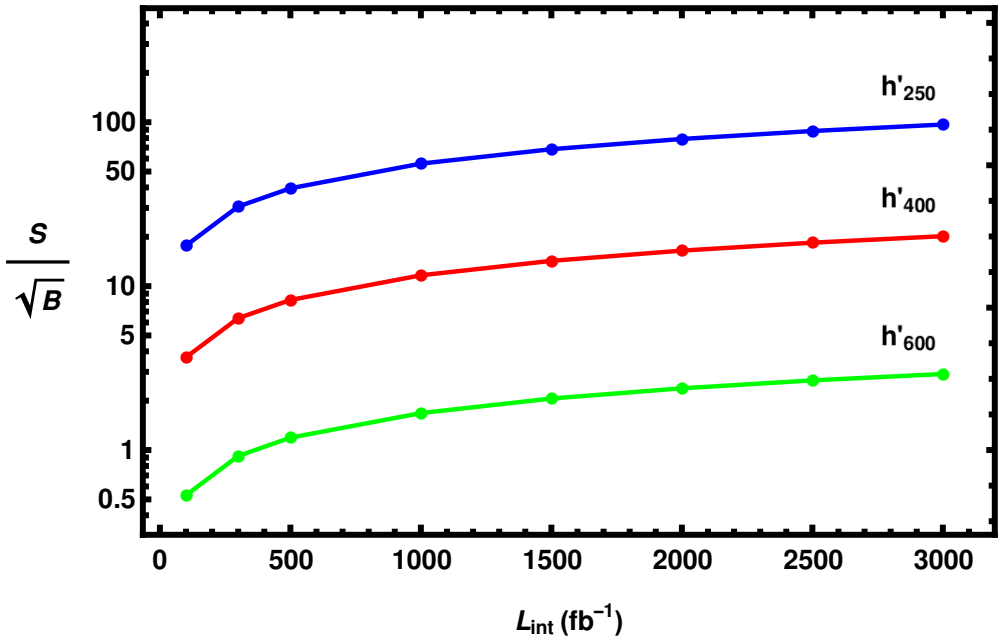

Figure 7: Significance of the $h' \to b\bar{b}\gamma\gamma$ signal of Fig. 5 and Fig. 6 relative to the background versus L_{int} at $m_{h'} = 250$ GeV (blue), 400 GeV (red) and 600 GeV (green). Data is produced at $\sqrt{s} = 14$ TeV and points are interpolated between values of $L_{\text{int}} = 100, 300, 500, 1000, 1500, 2000, 2500$ fb^{-1} and $L_{\text{int}} = 3000$ fb^{-1}. Event rates are computed with the cuts in Tab. 6 and the relative significance of the signals increases with L_{int}.

- Possibility of probing h' through its final decay into four charged leptons, along the process $pp \to h' \to ZZ \to 4\ell$ $(\ell = e,\ \mu)$ is shown by the following Feynman diagram

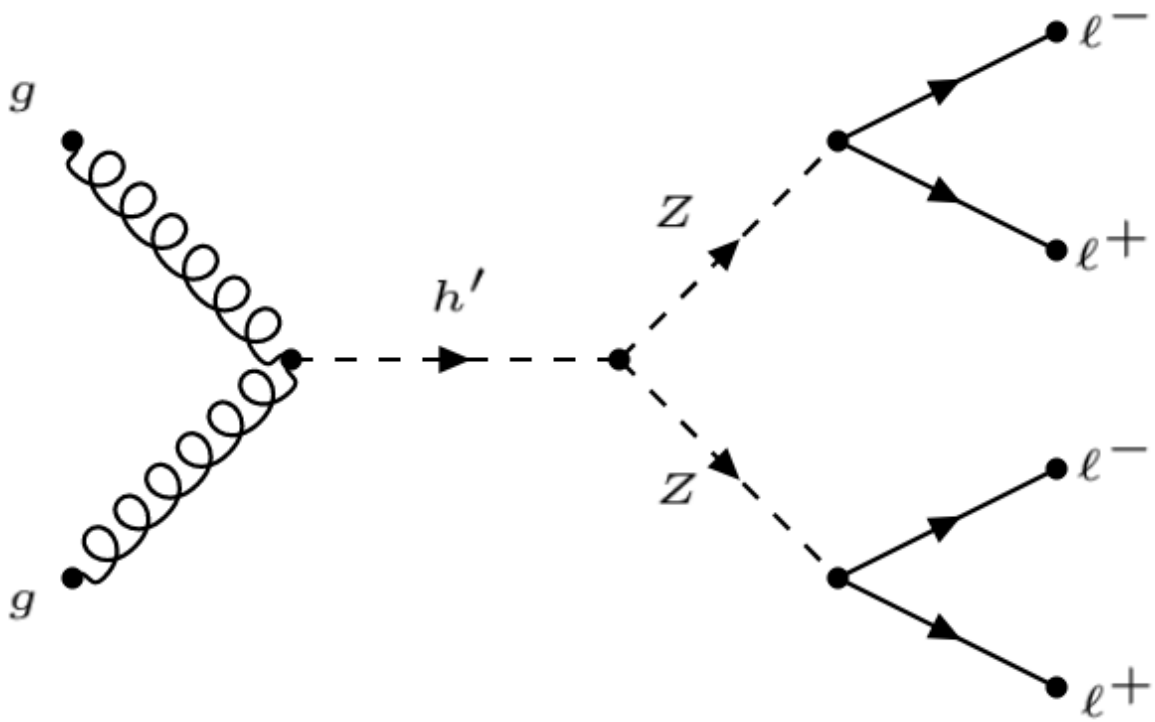

Figure 8: The ggF h'-production and decay $h' \to ZZ \to 4\ell$.

- In the narrow width approximation, the total cross section can be written as

$$\sigma(pp \to h' \to ZZ \to 4\ell) \approx \sigma(pp \to h') \times \text{BR}(h' \to ZZ) \times (\text{BR}(Z \to 2\ell))^2, \tag{34}$$

$m_{h'}$ (GeV)	$\sigma(pp \to h')$ (pb)	BR$(h' \to ZZ)$	$\sigma(pp \to h' \to ZZ \to 4\ell)$ (fb)
250	12.140	0.050	0.2428
400	5.050	0.025	0.0579

Table 8: $pp \to h'$ production cross section and its $h' \to ZZ$ decay branching ratio and the total cross section for its production and decay process $pp \to h' \to ZZ \to 4\ell$ for three different values of $m_{h'} = 250$ GeV and 400 GeV.

- With such small cross sections of Tab. 8 the number of associated events is extremely smaller than the relevant background, as shown in Fig. 9 (left). Thus, we consider larger $L_{\text{int}} = 3000$ fb^{-1} for the both cases of $m_{h'} = 250$ GeV and 400 GeV.
- Again, our signal is boosted away by the high mass value of the h' Higgs boson, an appropriate cut on the missing transverse hadronic energy $\not{H}_T = |-\sum_{\text{jet}} (\vec{P}_T)_{\text{jet}}|$ is applied as emphasized in Tab. 9 to enhance the relative significance of our signal to the corresponding irreducible background $pp \to 4\ell$.

Cuts (Select)	Signal (S): $m_{h'} = 250$ GeV (400 GeV)	Background (B)	S/$\sqrt{\text{B}}$
Initial (no cut)	728.00 (174.00)	79890.00	2.58000 (0.43000)
$\not{H}_T > 150.0$ GeV	58.65 ± 7.34 (38.20 ± 2.01)	247.70 ± 15.70	2.02457 ± 0.00790 (1.26340 ± 0

Table 9: Cut flow charts for the $h' \to ZZ \to 4\ell$ signal versus its relevant background and the corresponding number of events and significance at 3000 fb^{-1} and $\sqrt{s} = 14$ TeV for $m_{h'} = 250$ GeV, 400 GeV.

- After this cut we can see the significance of the signal increases over the relevant background

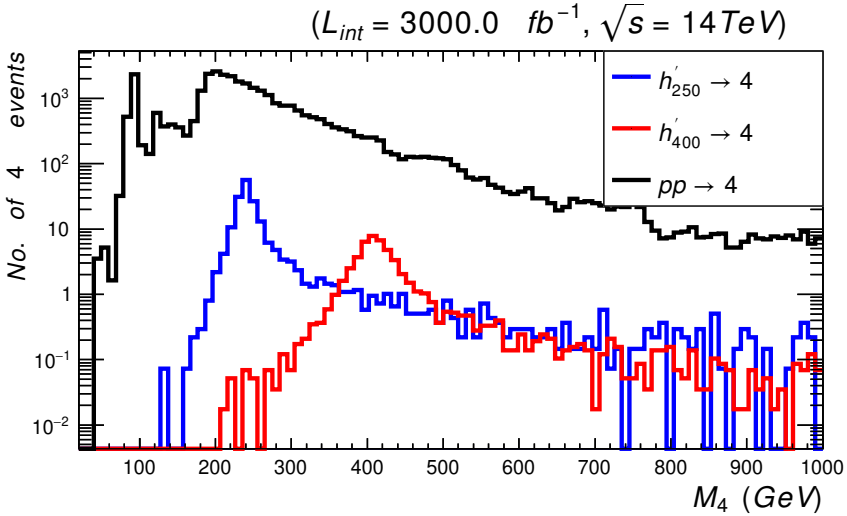

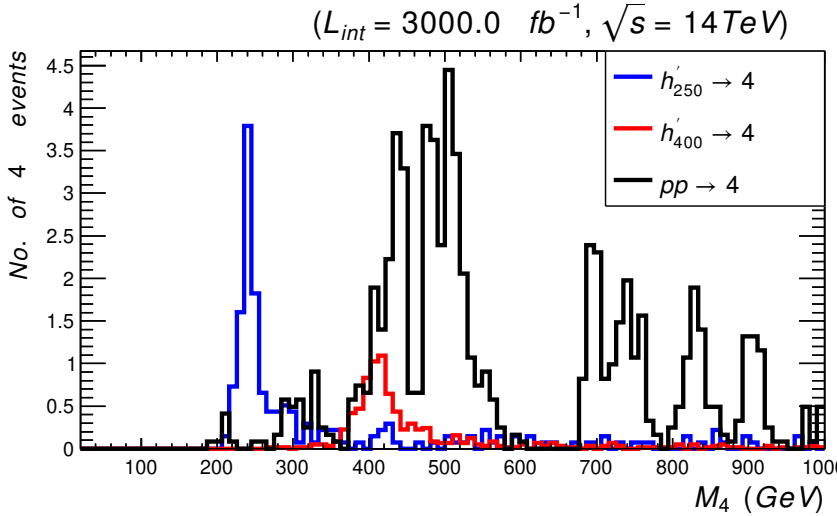

Figure 9: Number of signal events for $pp \to h' \to ZZ \to 4\ell$ decays at mass $m_{h'} = 250$ GeV (red) and 400 GeV (blue) induced by ggF versus the invariant mass of the final states 4ℓ, at $\sqrt{s} = 14$ TeV and $L_{\text{int}} = 3000$ fb^{-1} alongside with the relevant background events background (black) before (left) and after (right) applying the cut flow of Tab. 9. The corresponding values of cross sections and branching ratios are given in Tab. 8.

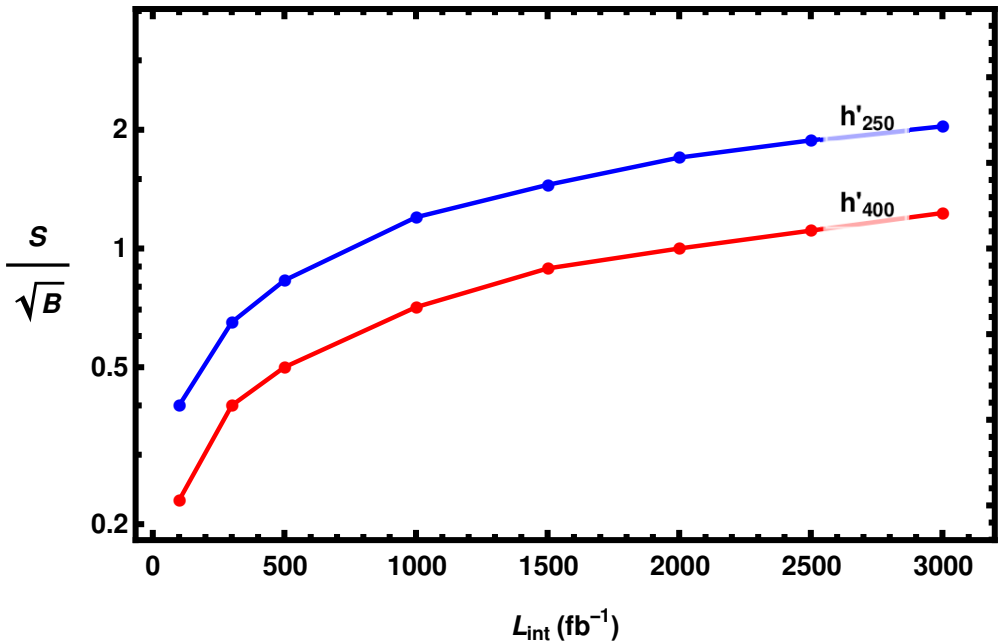

Figure 10: Significance of the $pp \to h' \to ZZ \to 4\ell$ signal of Fig. 9 relative to the corresponding background versus L_{int} at mass $m_{h'} = 250$ GeV (blue) and 400 GeV (red). Data is produced at $\sqrt{s} = 14$ TeV and points correspond to $L_{\text{int}} = 100, 300, 500, 1000, 1500, 2000, 2500$ fb^{-1} and $L_{\text{int}} = 3000$ fb^{-1}. Notice that event rates are computed after the cuts described in Tab. 9 and the relative significance of the signals increases with L_{int}.

Outline

- Proposal of a viable minimal left-right with neutrino masses inverse-seesaw mechanism.
- Full mass spectrum analysis in consistency with the experimental findings and limits.
- The next lightest Higgs, h', could of order a few hundred GeVs.
- We studied the LHC potential discovery for h' in this class of models. We performed analysis for searches for h' by looking for resonant peaks in the following two processes: $h' \to hh \to b\bar{b}\gamma\gamma$ and $h' \to ZZ \to 4\ell$ $(\ell = e, \mu)$.

- We considered three benchmark points, with $m_{h'} = 250$ GeV, 400 GeV and 600 GeV, at $\sqrt{s} = 14$ TeV and $L_{\text{int}} = 300$ fb^{-1} and $L_{\text{int}} = 3000$ fb^{-1}.
- We emphasized that h' can be probed with good statistical significances in di-Higgs channel, with $2\gamma + 2b$-jets final states.
- The channel of Z-pair production and decays to 4ℓ is much less significant and it may be observed only at very high $L_{\text{int}} = 3000$ fb^{-1} and for light h' with mass less than 300 GeV.

Outline

References I

[1] M. Ashry, K. Ezzat, and S. Khalil.
Search for Heavy Neutral Higgs Boson in Left-Right Model with Inverse-Seesaw at the LHC.
1 2021.

[2] N.G. Deshpande, J.F. Gunion, Boris Kayser, and Fredrick I. Olness.
Left-right symmetric electroweak models with triplet Higgs.
Phys.Rev., D44:837–858, 1991.

[3] Charanjit S. Aulakh, Alejandra Melfo, and Goran Senjanovic.
Minimal supersymmetric left-right model.
Phys.Rev., D57:4174–4178, 1998.

[4] Alessio Maiezza, Miha Nemevsek, Fabrizio Nesti, and Goran Senjanovic.
Left-Right Symmetry at LHC.
Phys. Rev. D, 82:055022, 2010.

[5] Debasish Borah, Sudhanwa Patra, and Utpal Sarkar.
TeV scale Left Right Symmetry with spontaneous D-parity breaking.
Phys.Rev., D83:035007, 2011.

[6] Miha Nemevsek, Goran Senjanovic, and Vladimir Tello.
Left-Right Symmetry: from Majorana to Dirac.
Phys.Rev.Lett., 110:151802, 2013.

[7] M. Ashry and S. Khalil.
Phenomenological aspects of a TeV-scale alternative left-right model.
Phys. Rev. D, 91(1):015009, 2015.
[Addendum: Phys.Rev.D 96, 059901 (2017)].

References II

[8] W. Abdallah, A. Awad, S. Khalil, and H. Okada.
Muon Anomalous Magnetic Moment and mu -> e gamma in B-L Model with Inverse Seesaw.
Eur. Phys. J. C, 72:2108, 2012.

[9] R.N. Mohapatra.
Mechanism for Understanding Small Neutrino Mass in Superstring Theories.
Phys. Rev. Lett., 56:561–563, 1986.

[10] M.C. Gonzalez-Garcia and J.W.F. Valle.
Fast Decaying Neutrinos and Observable Flavor Violation in a New Class of Majoron Models.
Phys. Lett. B, 216:360–366, 1989.

[11] Georges Aad et al.
Observation of a new particle in the search for the Standard Model Higgs boson with the ATLAS detector at the LHC.
Phys. Lett. B, 716:1–29, 2012.

[12] Serguei Chatrchyan et al.
Observation of a new boson at a mass of 125 GeV with the CMS experiment at the LHC.
Phys.Lett., B716:30–61, 2012.

[13] Morad Aaboud et al.
Search for pair production of Higgs bosons in the $b\bar{b}b\bar{b}$ final state using proton-proton collisions at $\sqrt{s} = 13$ TeV with the ATLAS detector.
JHEP, 01:030, 2019.

[14] Albert M Sirunyan et al.
Search for nonresonant Higgs boson pair production in the $\mathrm{b\bar{b}b\bar{b}}$ final state at $\sqrt{s} = 13$ TeV.
JHEP, 04:112, 2019.

Thank you!

Questions?